Chemical Science

ROYAL SOCIETY OF CHEMISTRY

EDGE ARTICLE

View Article Online
View Journal | View Issue

Cite this: *Chem. Sci.*, 2025, **16**, 22021

All publication charges for this article have been paid for by the Royal Society of Chemistry

Significant enhancement in the birefringence of metal phosphite halides *via* the introduction of π-conjugated cations

Ru-Ling Tang, * Yue Wang, Yi-Lei Lv, Bing-Wei Miao, Wenlong Liu and Sheng-Ping Guo *

Birefringent crystals have received increasing attention due to their extensive applications in the field of modern optics. While rationally designing excellent birefringent materials still remains challengeable, the emergence of organic–inorganic hybrid birefringent crystals has opened up new possibilities for high-performance birefringent crystals by combining the advantages of organic and inorganic components. Herein, two organic–inorganic hybrid zinc phosphite halides, $(C_4H_{12}N_2)[Zn_2(HPO_3)_2Cl_2]\cdot 2H_2O$ and $(C_5H_7N_2)[Zn(H_2PO_3)Cl_2]$, have been successively synthesized. $(C_4H_{12}N_2)[Zn_2(HPO_3)_2Cl_2]\cdot 2H_2O$ exhibits a three-dimensional (3D) structure constructed by unique hydrogen-bonded $\{[Zn_2Cl_2(HPO_3)_2(H_2O)_2]_\infty\}^{2-}$ lamellar, with non-π conjugated piperazine (PIP) cations $(C_4H_{12}N_2)^{2+}$ serving as counter cations. $(C_4H_{12}N_2)[Zn_2(HPO_3)_2Cl_2]\cdot 2H_2O$ reveals an ultraviolet (UV) cutoff edge below 200 nm and a small birefringence (0.01@546 nm) based on theoretical calculation. Considering the similar six-membered ring structures, we attempted to enhance birefringence performance by substituting non-π-conjugated piperazine with 4-aminopyridine featuring π-conjugation, and successfully obtained $(C_5H_7N_2)[Zn(H_2PO_3)Cl_2]$. It contains $[Zn(H_2PO_3)Cl_2]^-$ anions constructed by $[ZnO_2Cl_2]^{4-}$ and $[H_2PO_3]^-$ units, which form a one-dimensional (1D) structure with the isolated π-conjugated organic cations $(C_5H_6N_2)^+$ ($(4AMP)^+$). As a favourable result, the birefringence of $(C_5H_7N_2)[Zn(H_2PO_3)Cl_2]$ is enhanced to 0.378@546 nm based on experimental testing results, which is 37.8 times higher than that of $(C_4H_{12}N_2)[Zn_2(HPO_3)_2Cl_2]\cdot 2H_2O$, exceeding almost all phosphites and all commercially available birefringent crystals. Obviously, by converting the non-π conjugated piperazine to π-conjugated 4-aminopyridine units, a significant birefringence is achieved. First-principles theoretical studies confirm that the $(4AMP)^+$ cation makes a major contribution to the enhanced birefringence effect. The discovery of $(C_5H_7N_2)[Zn(H_2PO_3)Cl_2]$ indicates that organic–inorganic hybrid phosphite with planar π-conjugated groups has potential advantages in birefringent materials.

Received 5th July 2025
Accepted 13th October 2025

DOI: 10.1039/d5sc04977f

rsc.li/chemical-science

Introduction

Birefringent crystals are frequently employed as essential elements in optical manipulation and imaging detection. They are capable of achieving polarization control, phase modulation of light, and material structure analysis. As a result, they have aroused extensive concern in the field of optical materials.[1–8] Birefringent crystals currently accessible in the commercial market are mainly represented by MgF_2,[9] α-BaB_2O_4,[10] YVO_4,[11] TiO_2,[12] $LiNbO_3$,[13] and $CaCO_3$.[14] However, these materials are plagued by limitations such as a limited birefringence effect, crystalline quality issues, challenges in single-crystal growth, and a low laser damage threshold. Therefore, the rational design and synthesis of high-performance birefringent crystals remain a critical scientific and technological imperative.

Recently, organic–inorganic hybrid optical crystals have attracted increasing attention by incorporating the advantages of organic and inorganic components. By virtue of intermolecular synergistic effects and precise structural design, these crystals achieve multiple roles of "enhancement–regulation–expansion–optimization" in birefringent properties. The selection of organic components plays a critical role in regulating the optical anisotropy of materials. Based on the electronic arrangement of functional groups, structural building blocks can be classified into two categories: non-π-conjugated and π-conjugated types, which influence the electron polarizability and structural packing modes of crystals through distinct mechanisms. Numerous non-π-conjugated systems, such as borates $[(BO_4)^{5-}]$, phosphates, sulfates, and silicates, have been identified to exhibit good ultraviolet (UV) transparency.[15,16] However, the relatively weak structural anisotropy of regular tetrahedral moieties in phosphates/sulfates/silicates results in negligible birefringence, thereby hindering their applications

School of Chemistry and Chemical Engineering, Yangzhou University, 180 Siwangting Road, Yangzhou 225002, P. R. China. E-mail: rltang@yzu.edu.cn; spguo@yzu.edu.cn

as birefringent materials. The introduction of non-π-conjugated organic ligands, such as $(C_4H_{12}N_2)^{2+}$ (protonated piperazine cation), $(CH_3NH_3)^+$ (protonated methylamine cation), $(C_4H_{10}NO)^+$ (protonated morpholine cation), *etc.*, facilitate the formation of diverse and highly distorted metal-centered coordination polyhedra. This structural distortion is not merely a simple morphological change, but rather creates ideal conditions for the construction of open framework materials.[17–20] Representative compounds include $[HDMA]_2[ICl_2]\cdot Cl$ ($[HDMA]^+$ = protonated dimethylamine cation), $[HDMA]_2[IBr_2]\cdot Br$, $H_{11}C_4N_2CdI_3$, $CH_3NH_3GeBr_3$, *etc.*[21,22] Generally, planar structural groups with π-conjugation, such as trigonal $(BO_3)^{3-}$, $(NO_3)^-$, and $(CO_3)^{2-}$ anions, are favorable for birefringence.[23–25] In recent years, planar π-conjugated organic rings have attracted extensive attention due to their significant birefringence effects. For instance, organic groups including $(C_5H_6ON)^+$ (protonated 4-hydroxypyridine cation), $(H_2C_6N_9)^-$ (protonated tricyanomelonate anion), $(C_4H_6N_3)^+$ (protonated 2-aminopyrimidinium cation), $(C_3N_6H_7)^+$ (protonated melamine cation), $[H_xC_3N_3O_3]$ (x = 0, 1, 2, and 3) (protonated cyanuric acid), $(C_4N_3OH_6)^+$ (protonated 2-amino-4-hydroxypyrimidine cation), $(C_3N_2H_5)^+$ (protonated imidazole cation), $[C_{12}H_8N_2]$ (*ortho* phenanthroline), *etc.*, exhibit high optical activity and have been employed to construct high-performance birefringent crystals.[26–44]

For the inorganic component, we have chosen metal phosphite. Unlike phosphate, which features a rigid tetrahedral structure, it inherently exhibits optical anisotropy due to the strong covalent nature of its P–O bonds and the spatial orientation of its tetrahedral coordination. However, the minimal variations in P–O bond lengths within the PO_4 tetrahedron weaken the directionality of electron cloud distribution, resulting in generally low birefringence values for such materials. A critical challenge currently lies in how to effectively enhance birefringence through rational design of functional building blocks. In contrast, both $[HPO_3]^{2-}$ and $[H_2PO_3]^-$ units in phosphites are centered on phosphorus atoms to form polar asymmetric structures, and the central phosphorus atom is doubly bonded to one oxygen atom (P═O) and coordinates with hydroxyl oxygen atoms, endowing these structures with strongly polar P–O bonds and asymmetric electron cloud distributions.[45–47] Recent research studies have proved that phosphite compounds, such as $(C_{12}H_8N_2)SbF_2(H_2PO_3)$ (0.43@546 nm),[36] $K(GeHPO_3)_2Br$ (0.247@546 nm),[48] $(C_4H_6N_3)^+(H_2PO_3)^-$ (0.225@589.3 nm),[30] and $CsSn_2(HPO_3)_2I$ (0.200@546 nm), can exhibit large birefringence.[49] However, inorganic phosphite compounds currently face challenges arising from the inadequate birefringence activity (Δn < 0.3) of inorganic components and limitations in structural modulation. In contrast, organic–inorganic hybrid systems have broken through the performance ceiling of traditional inorganic materials *via* a synergistic model of "phosphite-group structural support and organic-ligand functional dominance", emerging as a research frontier in the field of birefringent crystals.[50–52] In organic–inorganic hybrid birefringent crystals, the value of phosphite groups lies in the dynamic regulatory capability endowed by their asymmetric structures—acting as "molecular scaffolds" to amplify the intrinsic optical anisotropy of organic ligands, rather than serving as optical active centers to directly generate large birefringence. To date, very few combinations of pseudo-tetrahedral phosphite groups and d^{10} metal cations have been reported. Among them, the electron configuration of Zn^{2+} features a completely filled d-orbital without unpaired electrons and shows coordination flexibility. Therefore, no d–d transitions occur in the visible to ultraviolet light range, avoiding light absorption loss. This provides a universal strategy for designing hybrid materials with both high transparency and large birefringence.[53,54] When Cl^- is introduced and combined with d^{10} metals, such a combination introduces lattice distortions and enhances optical anisotropy. Due to their highly polarizable nature, such combinations can induce large polarizability anisotropy, thereby significantly enhancing birefringence. Notably, Cl^- exhibits higher polarizability while maintaining superior optical transmittance across broad spectra compared to other halogen ions like Br^- and I^-. This can be attributed to the moderate ionic radius of Cl^-, where strong polarizability does not induce significant absorption losses, and balanced electrostatic interactions in coordination structures with d^{10} metals suppress scattering centers.[55,56]

Therefore, at first, this work attempts to incorporate non-π-conjugated piperazine (PIP) cations into a phosphite system to build a preliminary framework structure, successfully synthesizing one organic–inorganic hybrid zinc phosphite halide $(C_4H_{12}N_2)[Zn_2(HPO_3)_2Cl_2]\cdot 2H_2O$.[36] It exhibits a short UV cutoff edge (λ_{cutoff} < 200 nm). First-principles calculations reveal that it shows a small birefringence (0.01@546 nm). Furthermore, we adopted planar π-conjugated electrons of 4-aminopyridine cations $(4AMP)^+$ to replace PIP cations. By utilizing this organic group, we synthesized an organic–inorganic hybrid zinc phosphite halide $(C_5H_7N_2)[Zn(H_2PO_3)Cl_2]$ subsequently. Its experimental birefringence value astonishingly reaches 0.378@546 nm. First-principles theoretical studies confirm that the $(4AMP)^+$ cation makes a dominant contribution to the optical properties. Here, the syntheses, crystal structures, optical properties, theoretical calculations, and the structure–property relationship of $(C_4H_{12}N_2)[Zn_2(HPO_3)_2Cl_2]\cdot 2H_2O$ and $(C_5H_7N_2)[Zn(H_2PO_3)Cl_2]$ are systematically studied in this work.

Results and discussion

Crystal samples of $(C_4H_{12}N_2)[Zn_2(HPO_3)_2Cl_2]\cdot 2H_2O$ and $(C_5H_7N_2)[Zn(H_2PO_3)Cl_2]$ were obtained *via* the hydrothermal method and a simple aqueous solution process, respectively (see the SI for details). The powder X-ray diffraction (XRD) data have verified the phase purity of the samples (Fig. S1). Elemental analyses show the presence of C, N, Zn, Cl, P and O elements in $(C_4H_{12}N_2)[Zn_2(HPO_3)_2Cl_2]\cdot 2H_2O$ and $(C_5H_7N_2)[Zn(H_2PO_3)Cl_2]$ single crystals (Fig. S2), and the atomic ratios are very close to the stoichiometric ratios of the chemical formula. Cell parameters, along with corresponding bond lengths and bond angles of $(C_4H_{12}N_2)[Zn_2(HPO_3)_2Cl_2]\cdot 2H_2O$ and $(C_5H_7N_2)[Zn(H_2PO_3)Cl_2]$ are provided in Tables S1–S4.

$(C_4H_{12}N_2)[Zn_2(HPO_3)_2Cl_2]\cdot 2H_2O$ crystallizes in the monoclinic system with space group P_{21}/n (No. 14). The asymmetric

unit consists of one kind of $[HPO_3]^{2-}$ group, one unique Zn atom, one unique Cl atom, one kind of crystalline water molecule, and half a protonated piperazine cation $(C_4H_{12}N_2)^{2+}$. The Zn atom is coordinated by three O atoms and one Cl atom, forming a distorted ZnO_3Cl tetrahedron (Fig. 1a) with Zn–O bond lengths ranging from 1.9407(13) Å to 1.9615(14) Å and a Zn–Cl bond length of 2.2293(6) Å. The O–Zn–O bond angles vary from 100.24° to 108.01°, while the O–Zn–Cl bond angles range from 111.98° to 116.30°. The crystal structure features unique $\{[Zn_2Cl_2(HPO_3)_2(H_2O)_2]_\infty\}^{2-}$ layers (Fig. 1b and d), constructed by interconnected ZnO_3Cl and HPO_3 tetrahedra, as well as crystalline water molecules linked by hydrogen bonds, with an interlayer spacing of 8.05 Å. The alternating linkage between $[HPO_3]^{2-}$ and $[ZnO_3Cl]^{5-}$ units generates 8-membered channels (blue) and 4-membered channels (yellow). Crystalline water molecules are linked to O (2) atoms *via* O–H···O hydrogen bonds, filling the 8-membered channels, while protonated piperazine cations are alternately stacked between layers through N–H···O hydrogen bonds, forming a whole three-dimensional framework (Fig. 1c).

$(C_5H_7N_2)[Zn(H_2PO_3)Cl_2]$ belongs to the orthorhombic crystal system with the space group *Pccn* (No. 56). The asymmetric unit consists of one kind of $[H_2PO_3]^-$ group, one unique Zn atom, two unique Cl atoms, and one kind of planar π-conjugated organic $(C_5H_7N_2)^{2+}$ cation. The Zn atom is coordinated with Cl(1), Cl(2), O(2), and O(3) atoms, forming a tetrahedral $[ZnO_2Cl_2]^{4-}$ unit (Fig. 2a) with Zn–O bond lengths ranging from 1.9749(18) Å to 2.0096(17) Å and Zn–Cl bond lengths ranging from 2.2145(7) Å to 2.2436(8) Å. The O–Zn–O bond angle is 103.55(7)°, while the O–Zn–Cl bond angles range from 104.82(6)° to 108.86(5)°. The $[ZnO_2Cl_2]^{4-}$ unit and the $[H_2PO_3]^-$ unit are connected by sharing an O(2) atom to form $\{[Zn(H_2PO_3)Cl_2]_\infty\}^-$ single chains, where two single chains are linked *via* O–H···O hydrogen bonds to form double chains that are arranged along the *b*-axis in space (Fig. 2b), and the $(C_5H_7N_2)^+$ cations serve as counter ions to balance the charge (Fig. 2c). Notably, the protonated $(C_5H_7N_2)^+$ cations exhibit ordered regular arrangement, and they are arranged parallelly to the *a*-axis, while in the *bc* plane, they interdigitate in two alternating orientations, forming a dihedral angle of 38.84° (Fig. 2d). Such a relatively optimal arrangement contributes to enhance the birefringence. All bond lengths and angles observed in $(C_4H_{12}N_2)[Zn_2(HPO_3)_2Cl_2]\cdot 2H_2O$ and $(C_5H_7N_2)[Zn(H_2PO_3)Cl_2]$ are very similar to those found in other compounds.

So far, compounds combining piperazine with phosphite groups are extremely rare. In this study, $(C_4H_{12}N_2)[Zn_2(HPO_3)_2Cl_2]\cdot 2H_2O$ introduces piperazine as a structure-directing agent to regulate the formation of inorganic phosphite frameworks, constructing 8-membered channels and 4-membered channels with large-pore architectures. Similarly, $(C_4H_{12}N_2)[Zn_3(HPO_3)_4]$ also has a three-dimensional inorganic skeleton of $[Zn_3(HPO_3)_4]^{2-}$.[57] In contrast $(C_4H_{12}N_2)[Zn_2(HPO_3)_2Cl_2]\cdot 2H_2O$ exhibits $\{[Zn_2Cl_2(HPO_3)_2(H_2O)_2]_\infty\}^{2-}$ layers. The introduction of Cl^- ions enriches the structural diversity of the framework. Moreover, there is only one compound $(C_5H_7N_2)_2\cdot[Zn_3(HPO_3)_4]$ that combines $(C_5H_6N_2)$ with phosphite, and no research has been carried out on its birefringence properties.[58] In the structure of $(C_5H_7N_2)_2\cdot[Zn_3(HPO_3)_4]$, ZnO_4 tetrahedra and HPO_3

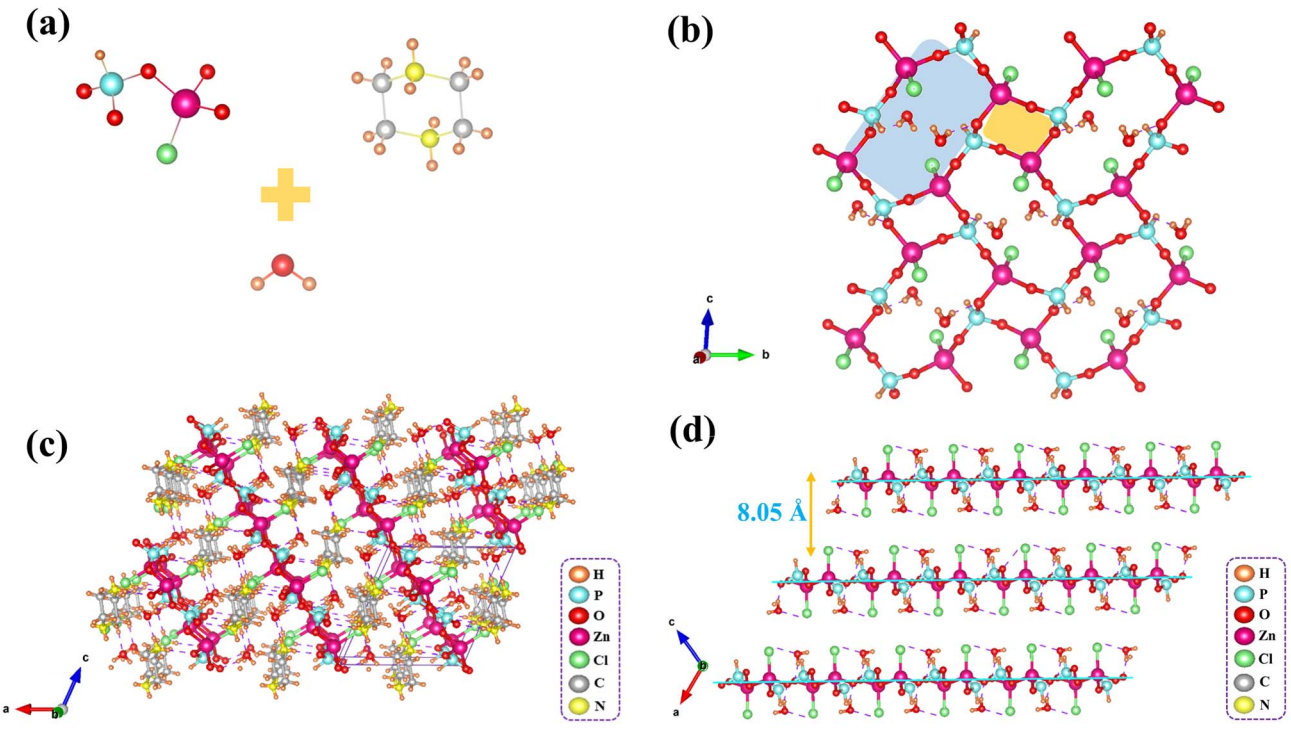

Fig. 1 (a) The $[Zn(H_2PO_3)Cl_2]^-$ unit, $(C_4H_{12}N_2)^{2+}$ cation and crystalline water molecules; (b) the $\{[Zn_2Cl_2(HPO_3)_2(H_2O)_2]_\infty\}^{2-}$ layer in the *bc* plane; (c) overall crystal structure viewed along the *b* direction; (d) the arrangement of the $\{[Zn_2Cl_2(HPO_3)_2(H_2O)_2]_\infty\}^{2-}$ layers along the *b*-axis.

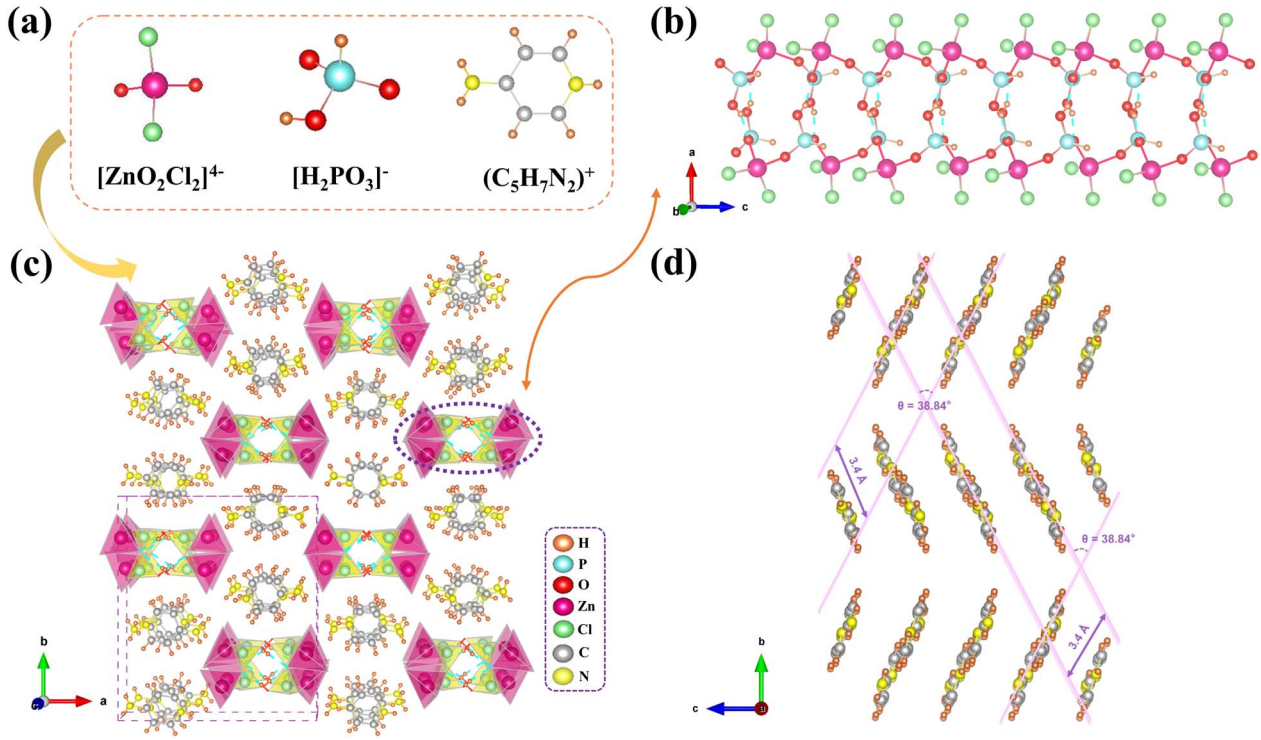

Fig. 2 The crystal structure of $(C_5H_7N_2)[Zn(H_2PO_3)Cl_2]$. (a) The $[ZnO_2Cl_2]^{4-}$, the $[H_2PO_3]^-$ unit, and the π-conjugated $(C_5H_7N_2)^+$ group; (b) the $\{[Zn(H_2PO_3)Cl_2]_\infty\}^-$ chains; (c) the whole crystal structure viewed from the *c* axis; (d) the π-conjugated $(C_5H_7N_2)^+$ groups viewed along the *b* axis and the dihedral angle between two alternating orientations.

pseudo-pyramids are connected to form $\{[Zn_3(HPO_3)_4]_\infty\}^{2-}$ layers containing 8-membered and 4-membered channels. Two protonated 4-aminopyridine cations are located in the channels, and interact with the host framework through the extensive hydrogen bonding, forming a three-dimensional open framework structure. This is different from the structure of $(C_5H_7N_2)[Zn(H_2PO_3)Cl_2]$, as it contains $\{[Zn(H_2PO_3)Cl_2]_\infty\}^-$ chains, and the introduction of Cl atoms enriches the structural diversity. In the phosphite system, $(C_5H_7N_2)[Zn(H_2PO_3)Cl_2]$ is the first compound in which the coordination of Zn shows $[ZnO_2Cl_2]^{4-}$ units. Currently, research on hybrid phosphite compounds containing d^{10} metal halides remains relatively limited. For instance $(C(NH_2)_3)_2Zn(HPO_3)_2$ exhibits a birefringence of only 0.030 at 1064 nm, and birefringence has not been investigated for most d^{10} metal halide-based hybrid phosphite compounds.[59] $(C_4H_{12}N_2)[Zn_2(HPO_3)_2Cl_2]\cdot 2H_2O$ and $(C_5H_7N_2)[Zn(H_2PO_3)Cl_2]$ in this study not only enrich the structural chemistry database of hybrid phosphites but also provide key scientific insights for subsequent function-oriented material design through the revelation of "structure–property" correlation mechanisms.

The UV-vis-NIR diffuse reflectance spectra of $(C_4H_{12}N_2)[Zn_2(HPO_3)_2Cl_2]\cdot 2H_2O$ and $(C_5H_7N_2)[Zn(H_2PO_3)Cl_2]$ (Fig. 3a and b) were measured, showing that both compounds belong to ultraviolet optical crystals. $(C_4H_{12}N_2)[Zn_2(HPO_3)_2Cl_2]\cdot 2H_2O$ shows an UV cutoff edge below 200 nm, indicating its potential application in the deep ultraviolet region. In a phosphite system, there are very few compounds with short UV cutoff edges, and recently reported optical materials include $(C(NH_2)_3)_2Zn(HPO_3)_2$ (194 nm),[59] $[Al_2(HPO_3)_3(H_2O)_3]\cdot H_2O$ (190 nm),[59] $Sc(HPO_3)(H_2PO_3)(H_2O)$ (<200 nm),[44] *etc.* The UV cutoff edge of $(C_5H_7N_2)[Zn(H_2PO_3)Cl_2]$ is 339 nm, and the experimental band gap corresponding to the Kubelka–Munk function is 3.66 eV (Fig. 3b). In π-conjugated compounds, the conjugated structure extends the scope of electron delocalization, reducing the energy gap between the highest occupied molecular orbital (HOMO) and the lowest unoccupied molecular orbital (LUMO), thereby leading to a smaller band gap. The infrared spectra of $(C_4H_{12}N_2)[Zn_2(HPO_3)_2Cl_2]\cdot 2H_2O$ and $(C_5H_7N_2)[Zn(H_2PO_3)Cl_2]$ in the wavelength range of 4000–400 cm^{-1} were analysed at room temperature (Fig. S3 and Table S6), and the attributions of infrared vibration peaks are consistent with previously reported compounds. The thermal stability analysis curve shows that $(C_4H_{12}N_2)[Zn_2(HPO_3)_2Cl_2]\cdot 2H_2O$ and $(C_5H_7N_2)[Zn(H_2PO_3)Cl_2]$ decompose at 120 °C and 108 °C, respectively (Fig. S6).

In order to investigate the structure–performance relationship of $(C_4H_{12}N_2)[Zn_2(HPO_3)_2Cl_2]\cdot 2H_2O$ and $(C_5H_7N_2)[Zn(H_2PO_3)Cl_2]$, the CASTEP package based on density functional theory (DFT) was used to calculate their electronic structure and optical properties. The calculated results show that the calculated bandgaps of $(C_4H_{12}N_2)[Zn_2(HPO_3)_2Cl_2]\cdot 2H_2O$ and $(C_5H_7N_2)[Zn(H_2PO_3)Cl_2]$ are 5.20 and 3.29 eV (Fig. S7a and b), respectively, smaller than the experimental values, which may be due to the limitation of the GGA calculation method. Therefore, in order to accurately analyze the optical properties of $(C_4H_{12}N_2)[Zn_2(HPO_3)_2Cl_2]\cdot 2H_2O$ and $(C_5H_7N_2)$

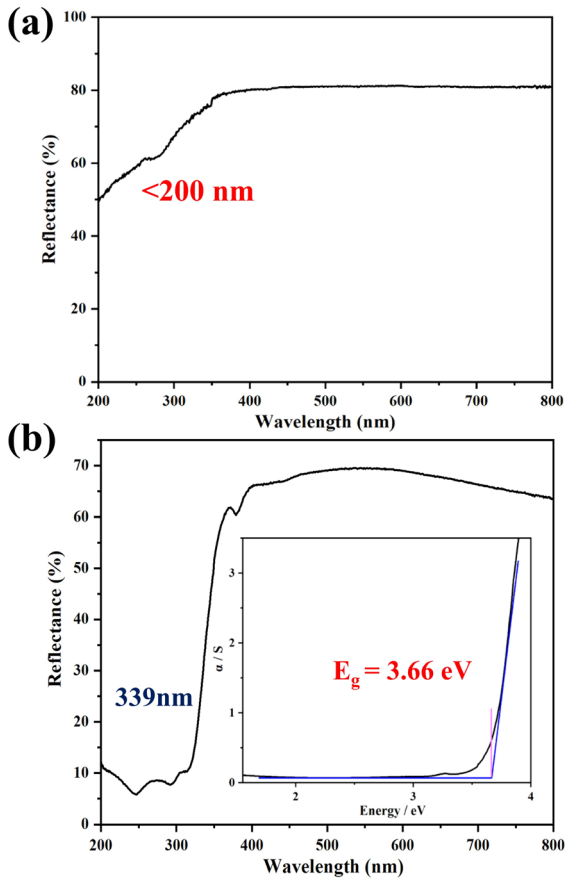

Fig. 3 (a) UV-vis-NIR diffuse reflectance spectrum of $(C_4H_{12}N_2)[Zn_2(HPO_3)_2Cl_2]\cdot 2H_2O$; (b) UV-vis-NIR diffuse reflectance spectrum and the optical band gap obtained from Tauc plots (inset) of $(C_5H_7N_2)[Zn(H_2PO_3)Cl_2]$.

$[Zn(H_2PO_3)Cl_2]$, scissor operators of 1 eV and 0.37 eV were conducted, respectively. The density of states (DOS) diagrams of $(C_4H_{12}N_2)[Zn_2(HPO_3)_2Cl_2]\cdot 2H_2O$ and $(C_5H_7N_2)[Zn(H_2PO_3)Cl_2]$ reveal their unique electronic structures. For $(C_4H_{12}N_2)[Zn_2(HPO_3)_2Cl_2]\cdot 2H_2O$, the DOS diagram shows that the top of the valence band is contributed by the Cl-3p, O-2p, and Zn-3d orbitals, while the Zn-4s and Zn-3p orbitals occupy the bottom of the conduction band. The results show that the optical properties of $(C_4H_{12}N_2)[Zn_2(HPO_3)_2Cl_2]\cdot 2H_2O$ are mainly affected by distorted $[ZnO_3Cl]$ tetrahedra.

For $(C_5H_7N_2)[Zn(H_2PO_3)Cl_2]$, the DOS diagram shows that the top of the valence band is contributed by the Cl-3p, N-2p, C-2p, O-2p and Zn-3d orbitals, while the C-2p and N-2p orbitals occupy the bottom of the conduction band (Fig. S8a and b). In addition, the C-2p and N-2p states of $(C_5H_7N_2)[Zn(H_2PO_3)Cl_2]$ occur near the top and bottom of the valence band, indicating that the delocalized π-conjugated $(C_5H_7N_2)^+$ cations have significant π–π conjugation effects. Moreover, the $[ZnO_2Cl_2]^{4-}$ tetrahedra also make a non-negligible contribution. Compared with $(C_4H_{12}N_2)^{2+}$, it can be seen that $(C_5H_7N_2)^+$ significantly affects optical properties. The calculated refractive indices for the two title compounds are depicted in Fig. 4c and S5, and the birefringence of $(C_4H_{12}N_2)[Zn_2(HPO_3)_2Cl_2]\cdot 2H_2O$ and $(C_5H_7N_2)[Zn(H_2PO_3)Cl_2]$ at 546 nm is 0.01 and 0.376, respectively. As a deep-ultraviolet transmission optical crystal $(C_4H_{12}N_2)[Zn_2(HPO_3)_2Cl_2]\cdot 2H_2O$ exhibits a small birefringence of 0.01@546 nm, demonstrating its potential as a zero-order waveplate material. The differential charge density (EDD) diagrams (Fig. 5a and b) show the charge transfer and ordered electron cloud distribution of Zn, Cl, and O atoms in the two compounds. In addition, the strong anisotropy and high stereochemical activity of the π-conjugated $(C_5H_7N_2)^+$ cations

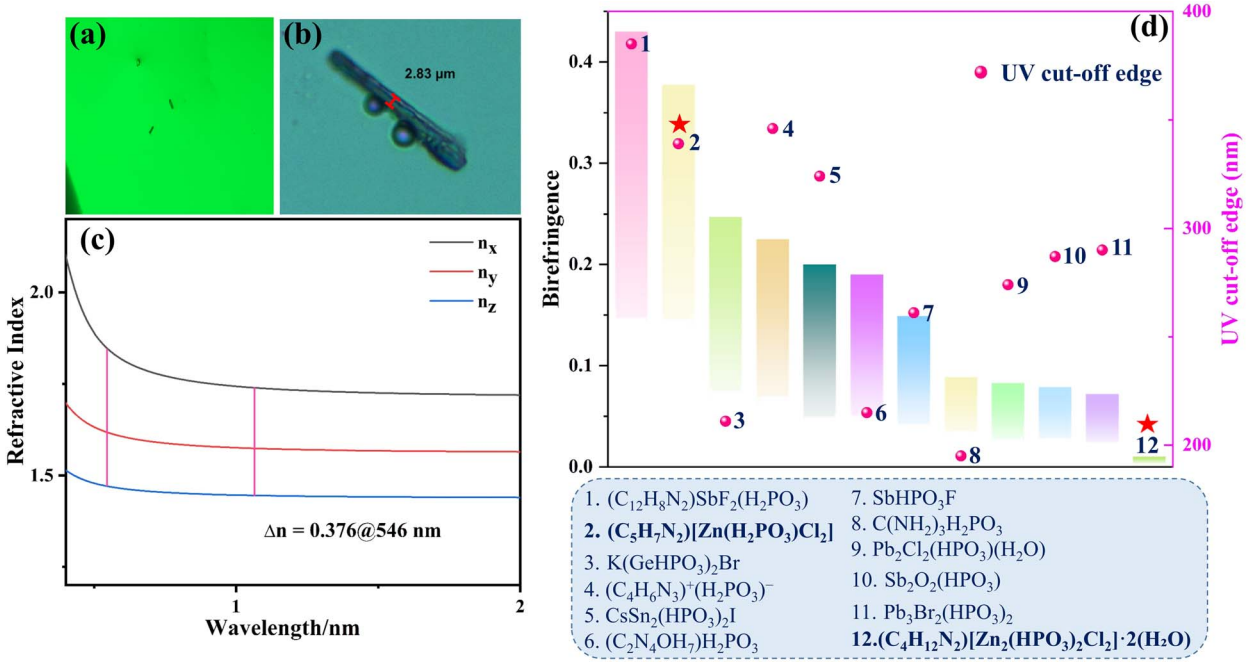

Fig. 4 (a) A single crystal exhibiting complete extinction. (b) Single crystal thickness. (c) Calculated refractive index dispersion curves of $(C_5H_7N_2)[Zn(H_2PO_3)Cl_2]$. (d) Comparison of birefringence and UV cut-off edge for representative phosphite crystals.

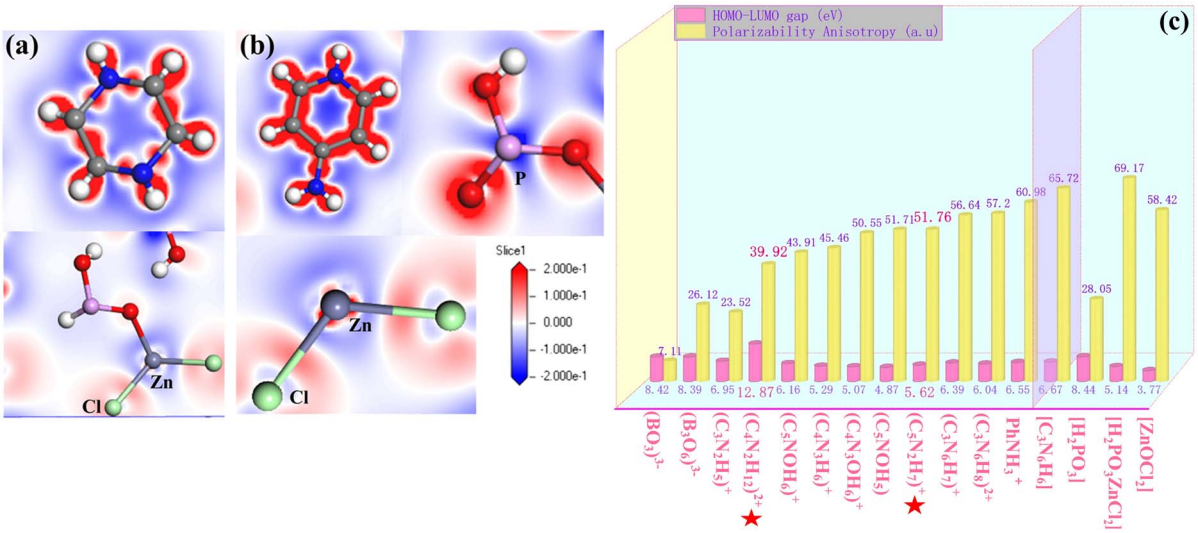

Fig. 5 (a and b) Electron-density difference map of $(C_4H_{12}N_2)[Zn_2(HPO_3)_2Cl_2]\cdot 2H_2O$ and $(C_5H_7N_2)[Zn(H_2PO_3)Cl_2]$. (c) The calculated polarizability anisotropy and HOMO–LUMO gap of the optically active groups and the inorganic moieties in $(C_5H_7N_2)[Zn(H_2PO_3)Cl_2]$.

and $[ZnO_2Cl_2]^{4-}$ anion contribute to the large birefringence of $(C_5H_7N_2)[Zn(H_2PO_3)Cl_2]$. In π-conjugated systems, electrons can move freely among multiple atoms. This delocalization causes a notable anisotropy in the electron-cloud distribution. That is to say, there are large disparities in how much the electron cloud extends in different directions. The piperazine molecule has an almost symmetrical six-membered ring structure, and its molecular shape is similar to a regular hexahedron. Due to this symmetrical shape, the orientation of the molecule in space has little effect on its optical properties. As a result, it is difficult for $(C_4H_{12}N_2)[Zn_2(HPO_3)_2Cl_2]\cdot 2H_2O$ to exhibit significant birefringence.

In order to further investigate the potential of $(C_5H_7N_2)[Zn(H_2PO_3)Cl_2]$ as a birefringent material, its birefringence was measured using a polarizing microscope equipped with a 546 nm light source. The thickness of the crystal was 2.83 μm, and the optical path difference at a wavelength of 546 nm was determined to be 1072.43 nm (Fig. 4a and b). According to the formula "$R = \Delta n \times T$", the birefringence can be calculated. The result shows that the birefringence of $(C_5H_7N_2)[Zn(H_2PO_3)Cl_2]$ at 546 nm is 0.378. A summary and comparison of the birefringence of phosphite-based compounds are provided in Table S7. Representative phosphite birefringent crystals are listed in Fig. 4d, revealing that $(C_5H_7N_2)[Zn(H_2PO_3)Cl_2]$ exhibits a birefringence value ranking the second among phosphite birefringent crystals, while when compared with $(C_{12}H_8N_2)SbF_2(H_2PO_3)$ and $(C_5H_7N_2)[Zn(H_2PO_3)Cl_2]$, it exhibits a shorter UV cutoff edge, implying its superior comprehensive optical properties. Up to now, only $(C_{12}H_8N_2)SbF_2(H_2PO_3)$[36] and $(C_5H_7N_2)[Zn(H_2PO_3)Cl_2]$ here exhibit birefringence values greater than 0.3 in a phosphite system. In comparison to the band gap of 3.20 eV of $(C_{12}H_8N_2)SbF_2(H_2PO_3)$, the band gap of $(C_5H_7N_2)[Zn(H_2PO_3)Cl_2]$ reaches 3.66 eV. Hence, $(C_5H_7N_2)[Zn(H_2PO_3)Cl_2]$ shows excellent comprehensive performance among phosphite birefringent materials. Additionally, the birefringence of $(C_5H_7N_2)[Zn(H_2PO_3)Cl_2]$ exceeds that of commercially available α-BaB_2O_4 (0.122@546 nm),[10] $CaCO_3$ (0.172@546 nm),[14] YVO_4 (0.204@532 nm),[11] and TiO_2 (0.306@546 nm).[12]

Inspired by the above research and strategies to improve structural anisotropy, we compared the polarizability anisotropy (δ) and HOMO–LUMO gaps of recently reported inorganic, organic π-conjugated, and non-π-conjugated groups with superior performance (Fig. 5c). Theoretical calculations show that the HOMO–LUMO gap of $(C_4H_{12}N_2)^{2+}$ reaches 12.87 eV, exceeding that of most inorganic and organic groups. Additionally, the $(C_5H_7N_2)^+$ cation exhibits remarkable polarizability anisotropy, surpassing that of most inorganic or organic π-conjugated groups such as $(BO_3)^{3-}$,[23] $(B_3O_6)^{3-}$,[60] $(C_3N_2H_5)^+$,[38] $(C_5NOH_6)^+$,[27] $(C_4N_3H_6)^+$,[30] $(C_4N_3OH_6)^+$,[33] and (C_5NOH_5) (Fig. 5c).[29] Notably, the anilinium cation $PhNH_3^+$ also exhibits an excellent HOMO–LUMO gap and remarkable polarizability anisotropy (δ), which demonstrates its significant potential for constructing high-performance birefringent materials. Therefore, in our subsequent work, we plan to incorporate $PhNH_3^+$ into phosphite systems to develop birefringent crystalline materials. It can be seen from these results that the $(C_5H_7N_2)^+$ cation significantly enhances birefringence. This directly demonstrates the significant contribution of $(C_5H_7N_2)^+$ groups to the optical anisotropy of $(C_5H_7N_2)[Zn(H_2PO_3)Cl_2]$. To further analyze the potential origin of birefringence in $(C_5H_7N_2)[Zn(H_2PO_3)Cl_2]$, we calculated the polarizability anisotropy (δ) and HOMO–LUMO gaps of the inorganic moieties in $(C_5H_7N_2)[Zn(H_2PO_3)Cl_2]$. Fig. 5c shows that the polarizability anisotropy of $[H_2PO_3ZnCl_2]$ also exhibits a remarkably large value. Hence, the synergistic interaction between the organic and inorganic components in $(C_5H_7N_2)[Zn(H_2PO_3)Cl_2]$ is effectively reflected in its comprehensive optical properties.[61] Through the complementarity of the organic cationic and inorganic anionic framework in terms of structural and electronic properties, the compound is collectively endowed with remarkable optical characteristics. Such intermolecular synergistic effects highlight the crucial role of organic–inorganic hybrid structures in

enhancing birefringence, endowing it with potential application value in the field of photonics materials.

Conclusions

In summary, we successfully synthesized two organic–inorganic hybrid zinc phosphite halides. $(C_4H_{12}N_2)[Zn_2(HPO_3)_2Cl_2]\cdot 2H_2O$ has a short UV cutoff edge. Replacing the non-π-conjugated piperazine with π-conjugated 4-aminopyridine results in a dramatic increase in birefringence of $(C_5H_7N_2)[Zn(H_2PO_3)Cl_2]$, surpassing all inorganic phosphites and all commercial birefringent crystals. Given the exceptional optical anisotropy of π-conjugated organic–inorganic hybrid phosphites, the birefringence enhancement strategy developed in this study provides feasible approaches for designing advanced birefringent materials based on π-conjugated structures. In the future, we will continue to deeply engage in this field, and continuously expand high-quality birefringence crystals in the π-conjugated system, thereby pioneering a new research model for advancing optical functional materials.

Data availability

CCDC 2463595 ($(C_4H_{12}N_2)[Zn_2(HPO_3)_2Cl_2]\cdot 2H_2O$) and 2463596 ($(C_5H_7N_2)[Zn(H_2PO_3)Cl_2]$) contain the supplementary crystallographic data for this paper.[62a,b]

Supplementary information (SI): experimental section, and additional tables and figures. See DOI: **https://doi.org/10.1039/d5sc04977f**.

Author contributions

This work was conceptualised by Ru-Ling Tang. Experimentation was performed by Ru-Ling Tang and Yue Wang. Software analysis was performed by Bing-Wei Miao. Yi-Lei Lv assisted with the experiments. Wenlong Liu contributed to supervision. Besides, Ru-Ling Tang contributed to funding acquisition and supervision. The first draft of the manuscript was prepared by Ru-Ling Tang and Yue Wang, and the final draft was edited by all the authors.

Conflicts of interest

The authors declare no competing financial interests.

Acknowledgements

The authors acknowledge the financial support from the National Natural Science Foundation of China (22101248), the Lvyangjinfeng Talent Program of Yangzhou (YZLYJFJH2021YXBS083), and the Qinglan Project of Yangzhou University.

Notes and references

1 T. Wu, X. Jiang, K. Duanmu, C. Wu, Z. Lin, Z. Huang, M. G. Humphrey and C. Zhang, *Adv. Sci.*, 2024, **11**, 2470070.
2 X. H. Meng, W. L. Yin and M. J. Xia, *Coord. Chem. Rev.*, 2021, **439**, 213916.
3 A. Tudi, S. Han, Z. Yang and S. L. Pan, *Coord. Chem. Rev.*, 2022, **459**, 214380.
4 Y. Q. Li, X. Zhang, J. Y. Zheng, Y. Zhou, W. Q. Huang, Y. P. Song, H. Wang, X. Y. Song, J. H. Luo and S. G. Zhao, *adv. Chem., Int. Ed.*, 2023, **62**, e202304498.
5 Y. Zhou, Z. F. Guo, H. G. Gu, Y. Q. Li, Y. P. Song, S. Y. Liu, M. C. Hong, S. G. Zhao and J. H. Luo, *Nat. Photonics*, 2024, **18**, 922–927.
6 J. Chen, M. B. Xu, H. Y. Wu, J. Y. Wu and K. Z. Du, *Angew. Chem., Int. Ed.*, 2024, **136**, e202411503.
7 W. F. Zhou and S. P. Guo, *Acc. Chem. Res.*, 2024, **57**, 648–660.
8 M. Mutailipu and S. L. Pan, *Angew. Chem., Int. Ed.*, 2020, **59**, 20302–20317.
9 M. J. Dodge, *Appl. Opt.*, 1984, **23**, 1980–1985.
10 X. J. Zhou Guoqing, X. Chen, H. Zhong, S. Wang, K. Xu, D. Peizhen and G. Fuxi, *J. Cryst. Growth*, 1998, **191**, 517–519.
11 T. T. H. T. Luo and E. L. Dereniak, *Opt. Lett.*, 2006, **31**, 616.
12 W. M. Sinton, *J. Opt. Soc. Am.*, 1961, **51**, 1309.
13 D. E. Zelmon, D. L. Small and D. Jundt, *J. Opt. Soc. Am. B*, 1997, **14**, 3319–3322.
14 G. Ghosh, *Opt. Commun.*, 1999, **163**, 95–102.
15 Z. Q. Chen, C. Y. Liu, Z. Li, J. J. Lu, J. J. Li, Z. H. Yang, S. L. Pan and M. Mutailipu, *Small*, 2025, **21**, 2504138.
16 Y. Li, J. H. Luo and S. G. Zhao, *Acc. Chem. Res.*, 2022, **55**, 3460–3469.
17 H. Y. Wu, C. L. Hu, M. B. Xu, Q. Q. Chen, N. Ma, X. Y. Huang, K. Z. Du and J. Chen, *Chem. Sci.*, 2023, **14**, 9533–9542.
18 R. Zhang, J. Fan, X. Zhang, H. Yu, H. Zhang, Y. Mai, T. Xu, J. Wang and H. J. Snaith, *ACS Photonics*, 2016, **3**, 371–377.
19 C. Y. Shen, D. F. Sun, Y. Y. Dang, K. Wu, T. X. Xu, R. X. Hou, H. Z. Chen, J. Y. Wang and D. L. Wang, *Inorg. Chem.*, 2022, **61**, 16936–16943.
20 R. L. Tang, D. X. Yang, L. Ma, Y. L. Lv, W. L. Long and S. P. Guo, *Adv. Opt. Mater.*, 2025, **13**, 2403044.
21 C. A. Chen, Y. Li, H. B. Huang, C. C. Jin, B. B. Zhang and K. M. Ok, *Angew. Chem., Int. Ed.*, 2025, **64**, e202506625.
22 Y. Liu, Y. P. Gong, S. N. Geng, M. L. Feng, D. Manidaki, Z. Deng, C. C. Stoumpos, P. Canepa, Z. Xiao, W. X. Zhang and L. L. Mao, *Angew. Chem., Int. Ed.*, 2022, **61**, e202208875.
23 X. L. Chen, B. B. Zhang, F. F. Zhang, Y. Wang, M. Zhang, Z. H. Yang, K. R. Poeppelmeier and S. L. Pan, *J. Am. Chem. Soc.*, 2018, **140**, 16311.
24 E. J. Cho, S. J. Oh, H. Jo, J. Lee, T. S. You and K. M. Ok, *Inorg. Chem.*, 2019, **58**, 2183.
25 G. H. Zou, H. Jo, S. J. Lim, T. S. You and K. M. Ok, *Angew. Chem., Int. Ed.*, 2018, **57**, 8619.
26 D. H. Lin, M. Luo, C. S. Lin, F. Xu and N. Ye, *J. Am. Chem. Soc.*, 2019, **141**(8), 3390.
27 J. Lu, X. Liu, M. Zhao, X. B. Deng, K. X. Shi, Q. R. Wu, L. Chen and L. M. Wu, *J. Am. Chem. Soc.*, 2021, **143**, 3647.
28 Y. Q. Li, X. Zhang, Y. Zhou, W. Q. Huang, Y. P. Song, H. Wang, M. J. Li, M. C. Hong, J. H. Luo and S. G. Zhao, *Angew. Chem., Int. Ed.*, 2022, **134**, e202208811.
29 Y. Li and K. M. Ok, *Angew. Chem., Int. Ed.*, 2024, **63**, e202409336.

30 Z. P. Zhang, X. Liu, X. M. Liu, Z. W. Lu, X. Sui, B. Y. Zhen, Z. S. Lin, L. Chen and L. M. Wu, *Chem. Mater.*, 2022, **34**, 1976–1984.
31 H. W. Jia, D. Xu, Z. J. Li, M. Arif, Y. S. Jiang and X. L. Hou, *Inorg. Chem. Front.*, 2024, **11**, 8331–8338.
32 J. Lu, Y. K. Lian, L. Xiong, Q. R. Wu, M. Zhao, K. X. Shi, L. Chen and L. M. Wu, *J. Am. Chem. Soc.*, 2019, **141**, 16151–16159.
33 M. Arif, X. Liu, Z. J. Li, H. W. Jia, Y. S. Jiang, Z. H. Yang, X. L. Hou and S. L. Pan, *Adv. Opt. Mater.*, 2025, **13**, 2402327.
34 Z. Y. Bai, J. Lee, H. Kim, C. L. Hu and K. M. Ok, *Small*, 2023, **19**, 2301756.
35 C. H. Hu, J. J. Liu, J. L. Qu, J. H. Hu and X. Z. Jiang, *J. Saudi Chem. Soc.*, 2024, **28**, 101789.
36 P. Zhang, X. H. Dong, L. Huang, Z. E. Lin, Y. Q. Zhou and G. H. Zou, *Angew. Chem., Int. Ed.*, 2025, **64**, e202424756.
37 R. L. Tang, W. Xu, W. J. Xie and C. L. Hu, *Inorg. Chem. Front.*, 2022, **9**, 5153–5160.
38 R. L. Tang, Y. L. Lv, L. Ma, B. W. Miao, W. L. Liu and S. P. Guo, *Chem. Sci.*, 2025, **16**, 4749.
39 P. F. Li, C. L. Hu, Y. F. Li, J. G. Mao and F. Kong, *J. Am. Chem. Soc.*, 2024, **146**, 7868–7874.
40 M. Mutailipu, J. Han, Z. Li, F. M. Li, J. J. Li, F. F. Zhang, X. F. Long, Z. H. Yang and S. L. Pan, *Nat. Photon.*, 2023, **17**, 694–701.
41 L. Qiu, L. Ma, W. L. Liu, Y. Y. Sun and R. L. Tang, *Adv. Opt. Mater.*, 2025, **13**, 2500149.
42 M. Yan, C. L. Hu, R. L. Tang, W. D. Yao, W. L. Liu and S. P. Guo, *Chem. Sci.*, 2024, **15**, 8500–8505.
43 M. Yan, R. L. Tang, W. D. Yao, W. L. Liu and S. P. Guo, *Chem. Sci.*, 2024, **15**, 2883–2888.
44 Z. C. Wu and S. P. Guo, *Coord. Chem. Rev.*, 2025, **542**, 216866.
45 L. Ma, Y. L. Lv, X. F. Ao, W. L. Liu, S. P. Guo and R. L. Tang, *Inorg. Chem.*, 2024, **63**, 7118–7122.
46 L. Ma, Y. L. Lv, B. W. Miao, G. R. Zhu, W. L. Liu, S. P. Guo and R. L. Tang, *Inorg. Chem. Front.*, 2025, **12**, 4804–4811.
47 G. X. Liu, R. L. Tang, L. Ma, Y. L. Lv, W. L. Liu and S. P. Guo, *Inorg. Chem.*, 2023, **62**, 1069–1074.
48 Y. Tian, W. Zeng, X. H. Dong, L. Huang, Y. Q. Zhou, H. M. Zeng, Z. E. Lin and G. H. Zou, *Angew. Chem., Int. Ed.*, 2024, **63**, e202409093.
49 L. Ma, W. Xu, L. Y. Y. Xu, Y. L. Lv, W. L. Liu, S. P. Guo and R. L. Tang, *Scr. Mater.*, 2024, **242**, 115913.
50 L. Qi, X. X. Jiang, K. N. Duanmu, C. Wu, Z. S. Lin, Z. P. Huang, M. G. Humphrey and C. Zhang, *J. Am. Chem. Soc.*, 2024, **146**, 9975–9983.
51 Y. Q. Zhang, Q. R. Ding, Y. Q. Li, X. Y. Song, W. Q. Huang, Y. Zhou, Q. P. Shao, Z. Y. Bai, S. G. Zhao and J. H. Luo, *Laser Photonics Rev.*, 2025, **19**, 2500368.
52 H. Zhou, M. Cheng, D. D. Chu, X. Liu, R. An, S. L. Pan and Z. H. Yang, *Angew. Chem., Int. Ed.*, 2025, **64**, e202413680.
53 H. X. Tang, Q. R. Shui, R. B. Fu, Z. Q. Zhou, W. X. Bao, Z. J. Ma and X. T. Wu, *J. Mater. Chem. C*, 2021, **9**, 16477–16484.
54 Q. H. Li, H. X. Mi, L. L. Yang, H. Y. Sha, D. L. Yang, Z. J. Wang, R. B. Su, B. Su and C. He, *J. Mater. Chem. C*, 2025, **13**, 10671–10675.
55 Y. G. Shen, M. L. Ding, G. Chen, Y. J. Luo, S. G. Zhao and J. H. Luo, *Small*, 2024, **20**, 2400549.
56 C. Y. Shen, C. Y. Zhang, Q. W. Xing, D. F. Sun, K. Wu, B. B. Zhang, J. Y. Wang and D. L. Wang, *Chem. Eng. J.*, 2025, **509**, 161389.
57 L. Wang, Z. Shi, W. S. Fu, G. H. Li, D. Zhang, W. J. Dong, Z. M. Dai, X. B. Chen and S. H. Feng, *J. Solid State Chem.*, 2004, **177**, 80–88.
58 Z. J. Dong, Y. Yan, W. Q. Zhang, Y. Wang and J. Y. Li, *Chem. Res. Chin. Univ.*, 2015, **31**, 498–502.
59 J. J. Zhang, X. M. Zhang, Y. Wang, K. Wu and B. B. Zhang, *Inorg. Chem.*, 2022, **61**, 18622–18628.
60 H. P. Wu, Z. J. Wei, Z. G. Hu, J. Y. Wang, Y. C. Wu and H. W. Yu, *Angew. Chem., Int. Ed.*, 2024, **63**, e202406318.
61 R. L. Tang, B. W. Miao, G. R. Zhu, W. L. Liu and S. P. Guo, *Adv. Sci.*, 2025, e15170.
62 (*a*) CCDC 2463595: Experimental Crystal Structure Determination, 2025, DOI: **10.5517/ccdc.csd.cc2npktr**; (*b*) CCDC 2463596: Experimental Crystal Structure Determination, 2025, DOI: **10.5517/ccdc.csd.cc2npkvs**.